Design, Realization and Testing of DC-DC Converter for Fuel Cell

Kirtibala Rathod
R&DE(E), DRDO
Pune, India
Email: kprathod.rde@gov.in

Prasad M. Naik
R&DE(E), DRDO
Pune, India
Email: pmnaik.rde@gov.in

Kiritkumar H. Vala
R&DE(E), DRDO
Pune, India
Email: kiritkumar.rde@gov.in

doi: https://doi.org/10.37285/bsp.SACAD2025.58

***Abstract*—Fuel cells are gaining prominence in clean energy systems because of their high efficiency, low emissions, and quiet operation. Despite these advantages, their inherent slow dynamic response and load-dependent output voltage present significant challenges for direct integration with electrical loads. To address these limitations, DC–DC converters are indispensable for effective power conditioning. However, existing converter topologies often involve trade-offs between efficiency, control flexibility, and system reliability. This paper presents the design, implementation, and experimental validation of a two-stage DC–DC converter specifically designed for fuel cell applications. The proposed architecture allows independent control of each stage, enabling precise voltage regulation, improved dynamic response, and stable power delivery under variable load condi- tions. Comprehensive simulation studies, supported by hardware prototype testing, confirm the converter's high efficiency and robust performance, thereby establishing its suitability for practical clean energy deployment.**

***Index Terms*—DC–DC converter, fuel cell, interleaved boost converter, phase-shifted full bridge converter**

I. Introduction

The growing demand for clean and sustainable energy has accelerated the adoption of fuel cells in transportation, stationary, and portable power applications [1]–[5]. Fuel cells are widely recognized for their high efficiency, low emissions, and silent operation, making them an attractive alternative to conventional energy sources [6], [7]. Despite these advantages, the electrical characteristics of fuel cells present integration challenges. Their output voltage is inherently low, highly dependent on load conditions, and nonlinear in nature, which limits direct utilization in most power electronic systems [4], [8]. To overcome these limitations, DC–DC converters play a crucial role in power conditioning the fuel cell output to meet the requirements of various loads and grid interfaces [9], [10]. By stepping up the low voltage to a suitable level, ensuring stable voltage regulation, and providing improved transient response, these converters enable effective utilization of the fuel cell. In addition, they enhance overall system performance by supporting hybrid operation with energy storage devices such as batteries or supercapacitors, thereby improving reliability and efficiency in practical applications [11].

Various DC–DC converter topologies have been proposed and investigated in the literature for fuel cell applications [12]–[18]. These topologies are broadly classified into non-isolated and isolated converter structures, depending on whether galvanic isolation is provided between the fuel cell and the load.

Non-isolated converters, such as boost and buck–boost configurations, offer high efficiency and compact design. However, they are limited in achieving high voltage gain and often exhibit significant input current ripple [19]. To overcome these issues, multilevel boost converters have been proposed to enhance voltage gain [20], [21], while multiphase interleaved boost converters mitigate input ripple and thereby reduce fuel cell degradation [22]. Several interleaved topologies have also been reported and reviewed [12]. Despite these advancements, the absence of galvanic isolation exposes systems to ground faults and reduces reliability. To address this, isolated topologies such as full-bridge, half-bridge, and resonant converters are used which provide galvanic isolation and improved safety, but at the expense of higher circuit complexity, component count, and implementation cost [13]. Thus, the choice between non-isolated and isolated converters involves a trade-off among efficiency, reliability, and compactness.

In a single-stage converter, the required output voltage is typically regulated by controlling the gate signals through PWM, phase-shift, or frequency modulation, depending on the operating requirements [23]. However, relying solely on this single control variable may not provide sufficient flexibility to accommodate wide source and load variations. Furthermore, although the literature extensively addresses the progression from design to realization and testing, most reported works remain limited to laboratory-scale prototypes, with limited emphasis on the development and validation of field-deployable systems.

This paper presents the design, realization, and testing of a two-stage DC–DC converter specifically intended for fuel cell applications. The proposed topology enables enhanced control flexibility through independent regulation of both stages, while ensuring high efficiency and reliable operation under varying load and operating conditions. The design methodology incorporates analytical modeling, simulation studies, hardware implementation, and experimental validation. The results demonstrate that the developed converter not only satisfies the operational requirements of fuel cell systems but also exhibits strong potential for deployment in practical clean energy applications.

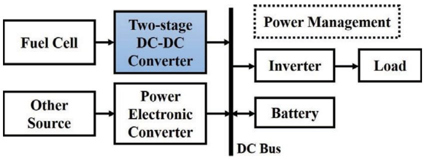

Fig. 1: Block diagram of Hybrid Energy System

II. System Description and Design

A typical fuel-cell embedded hybrid energy system is shown in Fig. 1, where the fuel cell and other power sources such as solar PV and/or wind turbine are connected to the DC bus through power electronic converters. As the dynamic response of the fuel cell is relatively poor and renewable sources exhibit uncertainty, buffer energy storage in the form of a battery is required. The load is supplied through an inverter, while the power management system ensures coordinated control and communication among all subsystems.

The design inputs for the proposed two-stage DC–DC converter are derived from the specifications of fuel cell stack and the battery. Being a Polymer Electrolyte Membrane (PEM) fuel cell, the measured open-circuit voltage of a single cell is 0.96 V, which drops to 0.60 V at rated power. In a modular configuration with four stacks, a total of 620 cells are connected in series, resulting in a fuel cell output voltage that varies between 372–595 V from no-load to rated power. Under overload conditions, the stack voltage may decrease further due to increased current demand. Considering these operating conditions, the input voltage range for the two-stage DC–DC converter is selected as 250–600 V.

On the output side, the battery has a nominal voltage of 288 V, with variation between 225–330 V from discharge to charge states. This defines the required DC–DC converter output voltage range. Based on the rated power of the fuel cell, a 46 kW DC–DC converter is required. To achieve modularity and ease of control, two identical 23 kW converters operating in parallel are proposed. The key specifications of the DC–DC converter are summarized in Table I.

TABLE I: DC–DC Converter Specifications

Electrical Parameters	Ratings
Power	2 × 23 kW
Input Voltage	250–600 V
Output Voltage	225–330 V
Output Voltage Ripple	<1%
Efficiency	90%

To ensure low input ripple current and high efficiency, an interleaved boost converter is connected at the fuel cell stack side. The boost stage regulates the DC bus voltage to 600 V. Furthermore, safety and fault tolerance are critical requirements in end-use applications, making galvanic isolation mandatory. This is achieved using a full-bridge converter. The schematic diagram of the overall system is shown in Fig. 2.

The design of a two-phase interleaved boost converter is discussed in [24]. For a three-phase interleaved boost converter, the critical inductance and the minimum output capacitance required to satisfy the voltage ripple specification are calculated using

$$L_{\text{crit,phase}} = \frac{3\,D_{\max}\,(1 - D_{\max})^2\,R}{2 f_s} \quad (1)$$

$$C \geq \frac{I_O\,D_{\max}}{3 f_s\,\Delta V_{\text{req}}} \quad (2)$$

where R is the equivalent load resistance, I_O is the output current, $f_s (12\ kHz)$ is the switching frequency, $D_{\max}$ is the maximum duty cycle, and ΔV_{req} is the allowable peak-to-peak voltage ripple. Substituting the design values, the calculations yield a duty cycle of $D_{\max} = 0.583$ and an output current of $I_O = 38.3$ A. From (1) and (2), the required critical inductance per phase is 198 µH, while the minimum output capacitance is 103 µF for 1% voltage ripple. This value also satisfy the ripple current requirement.

For the phase-shifted full-bridge (PSFB) converter, the boundary inductance and the minimum output capacitance required to satisfy the ripple specification are expressed as

$$L_b = \frac{(1 - 2D_{\text{eff}})\,R}{4 f_s} \quad (3)$$

$$C_{\min} = \frac{(1 - 2D_{\text{eff}})\,V_O}{32\,V_r\,L f_s^2} \quad (4)$$

where D_{eff} denotes the effective duty cycle (phase-shift power-transfer window, $0 \leq D_{\text{eff}} \leq 0.5$) and R is the load resistance with a switching frequency of $25\ kHz$. Using the design parameters with the lowest power considered as one-tenth of the rated load, near the battery full-charge voltage of 330 V, the required boundary inductance and minimum capacitance from (3)–(4) are calculated as 55 µH and 10.6 µF, respectively, ensuring compliance with the voltage ripple specification.

III. Simulation

To validate the analytical design and verify the steady-state as well as dynamic performance of the proposed two-stage DC–DC converter, detailed circuit-level simulations are carried out in PSIM. The simulations are performed using ideal device models and the design parameters derived in Section II. The overall objective of the simulations is to examine the operating waveforms, verify compliance with specifications, and evaluate the controller performance under different load conditions.

A. Stage 1: Interleaved Boost Converter

The first stage, a three-phase interleaved boost converter, is simulated with an input voltage of 250 V, an inductance of 230 μH per phase, and full-load power of 23 kW. Fig. 3 shows the simulated waveforms of the gate signals, inductor current, and output voltage. The results confirm that the converter operates in continuous conduction mode (CCM). The inductor currents are phase-shifted by 120°, resulting in

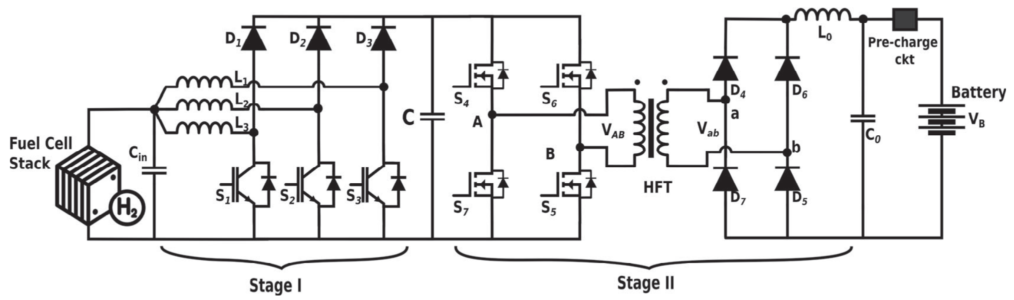

Fig. 2: Schematic of two-stage DC-DC converter

effective cancellation of ripple at the input and output. The measured output voltage ripple is less than 0.5%. These results validate the analytical design.

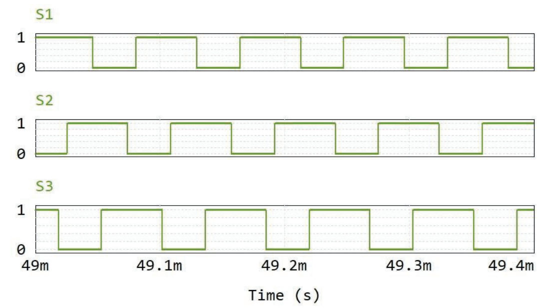

(a) Gate signals

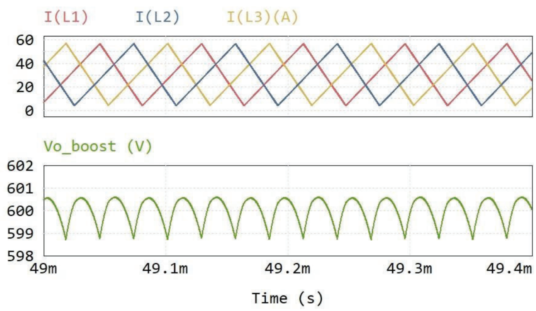

(b) Inductor current and output voltage

Fig. 3: Simulation results of the interleaved boost converter

B. *Stage 2: Phase-Shifted Full Bridge Converter*

The regulated 600 V DC bus from the boost stage is supplied to the second stage, a Phase-Shifted Full Bridge (PSFB) converter. The effective output power is controlled by adjusting the phase shift between the leading and lagging legs of the full bridge. Fig. 4 illustrates the simulated gate signals, transformer primary voltage, output inductor current, and output voltage for a phase shift of 56°. It can be observed that the applied transformer voltage varies according to the phase shift, and the resulting inductor current and output voltage exhibit smooth waveforms with voltage ripple less than 0.5%. This demonstrates the suitability of phase-shift control for regulating power flow in the proposed system.

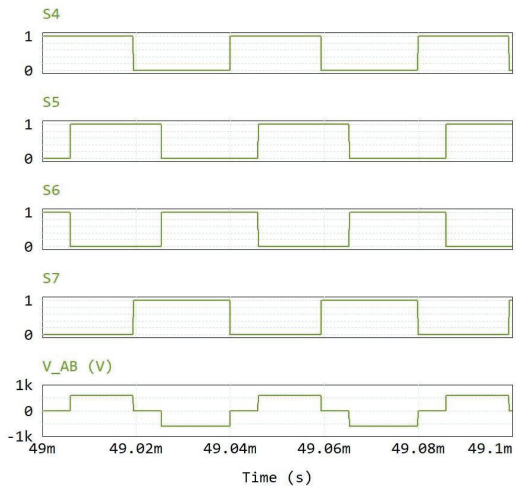

(a) Gate signals and transformer primary voltage

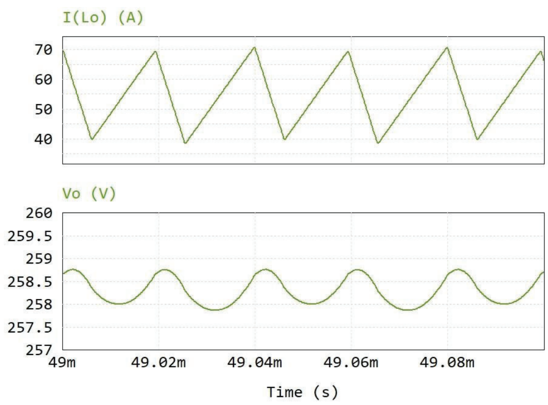

(b) Inductor current and output voltage

Fig. 4: Simulation results of the Phase-Shifted Full Bridge (PSFB) converter

C. Closed-Loop Performance with CC–CV Charging

On the output side, the DC bus is interfaced with a battery energy storage system that requires charging in constant-current (CC) and constant-voltage (CV) modes. To achieve this, the overall two-stage converter is operated under closed-loop control. PI controllers are implemented for both current and voltage regulation, as shown in Fig. 5.

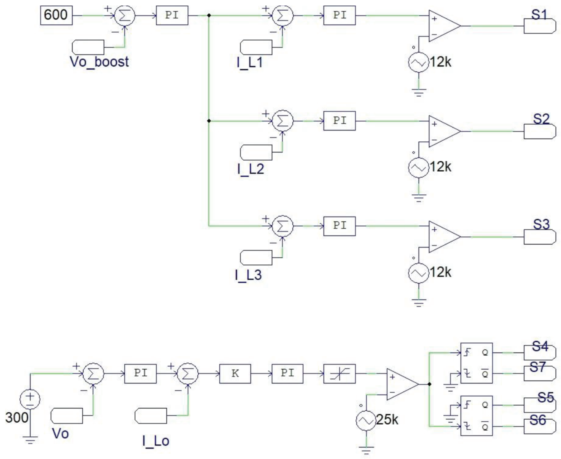

Fig. 5: Closed-loop control structure for the proposed two-stage DC–DC converter

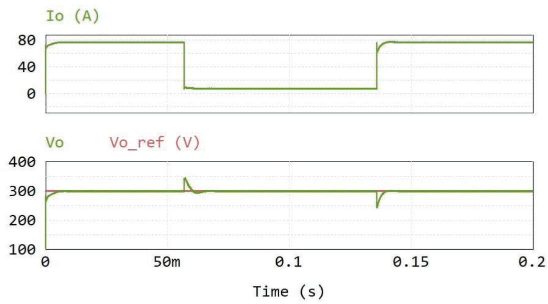

Fig. 6: Closed-loop response: voltage, current, and load variation

The corresponding dynamic response under varying load and voltage conditions is shown in Fig. 6. The results indicate that the proposed control strategy ensures stable operation for different load conditions. Further, it can also be operated CC mode by having reference current generation instead of calculating from voltage loop.

IV. Hardware Realization, Testing, and Results

The proposed two-stage DC–DC converter has been realized in hardware to validate the design and simulation results. The block diagram of the hardware setup is shown in Fig. 7, which consists of both power and control circuits along with auxiliary subsystems. The corresponding realized hardware is illustrated in Fig. 8.

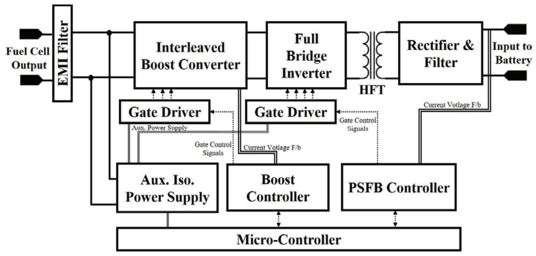

Fig. 7: Block diagram for hardware realization of the two-stage DC–DC converter

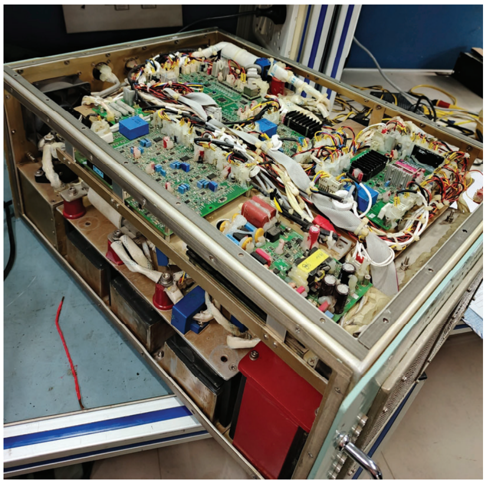

Fig. 8: Realized two-stage DC–DC converter prototype

The power stage comprises a three-phase interleaved boost converter, a phase-shifted full-bridge (PSFB) inverter, a high-frequency transformer (HFT), and a secondary-side rectifier with an output filter. The boost converter employs three parallel legs with MOSFET switches and ferrite-core inductors, sharing the input power equally and minimizing current ripple through interleaving. The PSFB stage regulates the power flow via phase-shift modulation and enables zero-voltage switching (ZVS). A custom-designed HFT with litz-wire windings provides galvanic isolation while reducing AC losses. The rectifier and LC filter stage ensure a low-ripple DC output suitable for battery charging.

The control stage is built around a microcontroller that coordinates both converter stages under closed-loop operation. A current-mode controller regulates the DC bus voltage on the boost side, while the PSFB is controlled using phase-shift modulation. Constant-current and constant-voltage (CC–CV) charging is achieved through PI controllers. Isolated gate drivers and auxiliary SMPS supplies provide reliable operation of the power stage, while feedback sensors ensure accurate control and fault protection.

To evaluate performance, the converter was first tested independently at its rated capacity using a grid-connected rectifier as input and a resistive load at the output. Incremental load steps were applied to examine the response, and key parameters such as input/output voltage, current, ripple, efficiency, and voltage stability were measured. The recorded step-load response is shown in Fig. 9, confirming that the system maintains stable operation across varying loads.

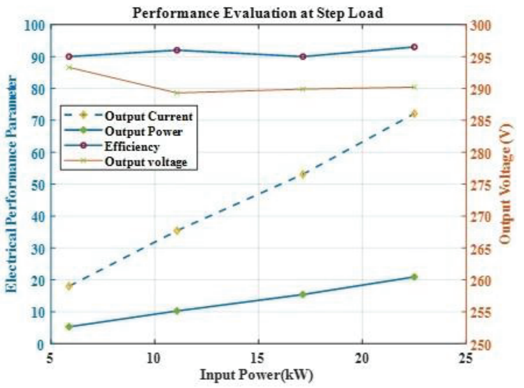

Fig. 9: Experimental step-load response of the proposed converter

A long-duration heat run test was then performed by operating the converter continuously for 12 hours at rated power. As illustrated in Fig. 10, the system exhibited good thermal stability and sustained efficiency, validating the robustness of the hardware design.

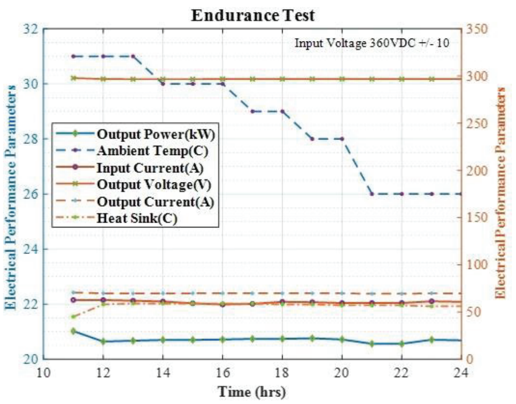

Fig. 10: Heat run test results over continuous 12-hour operation

Finally, system-level validation was carried out by integrating the converter with a practical fuel cell and battery bank. The overall performance under this hybrid configuration, including both steady-state and transient responses, is summarized in Tab.. II. The results confirm that the proposed converter ensures reliable power transfer and effective in real-world applications.

TABLE II: Converter Performance Data

Parameter	Value
Input Voltage, V_{in} (V)	365
Input Current, I_{in} (A)	62.5
Input Power, P_{in} (W)	22812.5
Output Voltage, V_{out} (V)	290.2
Output Current, I_{out} (A)	72.1
Output Power, P_{out} (W)	20923
Efficiency (%)	91.71
Output Ripple (mV, p-p)	680

V. Conclusion

This paper presented the practical design and implementation of a two-stage DC–DC converter for fuel cell applications, progressing from analytical calculation and simulation to complete hardware realization and testing. The proposed converter architecture effectively minimizes voltage ripple, provides galvanic isolation, and supports flexible control of both source and load dynamics. Zero-voltage switching (ZVS) in the PSFB stage significantly reduces switching losses, contributing to enhanced efficiency. The system was comprehensively evaluated through step-load response tests, long-duration heat runs, and integration with a real fuel cell and battery bank. Results confirm that the converter achieves stable operation, efficient power transfer, and reliable closed control operations.

Future work may focus on further optimization of the system to increase power density, enhance control strategies, and improve overall conversion efficiency.

VI. Acknowledgement

The authors gratefully acknowledge the support provided by M/s Grow Control Power Tech and M/s L&T Limited for their valuable support in hardware realization and testing of the converter system.

References

[1] N. A. A. Qasem and G. A. Q. Abdulrahman, "A recent comprehensive review of fuel cells: History, types, and applications," *International Journal of Energy Research*, vol. 2024, no. 1, p. 7271748.

[2] M. A. Aminudin, S. Kamarudin, B. H. Lim, E. Majilan, M. S. Masdar, and N. Shaari, "An overview: Current progress on hydrogen fuel cell vehicles," *International Journal of Hydrogen Energy*, 2022.

[3] R. Rath, P. Kumar, S. Mohanty, and S. Nayak, "Recent advances, unsolved deficiencies, and future perspectives of hydrogen fuel cells in transportation and portable sectors," *International Journal of Energy Research*, vol. 43, pp. 8931 – 8955, 2019.

[4] J. Lai and M. Ellis, "Fuel cell power systems and applications," *Proceedings of the IEEE*, vol. 105, pp. 2166–2190, 2017.

[5] V. Cigolotti, M. Genovese, and P. Fragiacomo, "Comprehensive review on fuel cell technology for stationary applications as sustainable and efficient poly-generation energy systems," *Energies*, 2021.

[6] M. J. B. Kabeyi, "Fuel cells design, operations and applications," in *Proceedings of the International Conference on Industrial Engineering and Operations Management*, September 12, 2023, 2023.

[7] S. V. Guaitolini, I. Yahyaoui, J. Fardin, L. Encarnac¸a˜o, and F. Tadeo, "A review of fuel cell and energy cogeneration technologies," *2018 9th International Renewable Energy Congress (IREC)*, pp. 1–6, 2018.

[8] G. Subramaniam, C. Kumar, and F. Alsaif, "Performance evaluation of fuel cell based on a dc-dc boost converter through optimized mppt controller," *Frontiers in Energy Research*, 2024.
[9] A. Kolli, A. Gaillard, A. D. Bernardinis, O. Be´thoux, D. Hissel, and Z. Khatir, "A review on dc/dc converter architectures for power fuel cell applications," *Energy Conversion and Management*, vol. 105, pp. 716–730, 2015.
[10] Y. Zhang, H. Liu, J. Li, M. Sumner, and C. Xia, "Dc–dc boost converter with a wide input range and high voltage gain for fuel cell vehicles," *IEEE Transactions on Power Electronics*, vol. 34, pp. 4100–4111, 2019.
[11] M. Marchesoni and C. Vacca, "New dc–dc converter for energy storage system interfacing in fuel cell hybrid electric vehicles," *IEEE Transactions on Power Electronics*, vol. 22, pp. 301–308, 2007.
[12] F. A. Abbas, T. A. Abdul-Jabbar, A. A. Obed, A. Kersten, M. Kuder, and T. Weyh, "A comprehensive review and analytical comparison of non-isolated DC-DC converters for fuel cell applications," *Energies*, vol. 16, no. 8, 2023.
[13] A. Rehman, S.-W. Ryu, H. Park, and J.-W. Jung, "A critical review of recent industrial developments, trends, and future perspectives of power electronic systems: Fuel cell electric vehicles," *IEEE Transactions on Industrial Informatics*, vol. 20, pp. 6060–6074, 2024.
[14] D. N. Jayachandran, J. Sathik, T. Padhi, and A. Kumari, "A comprehensive review of the quadratic high gain dc-dc converter for fuel cell application," *International Journal of Electronics and Telecommunications*, vol. 68, no. 2, pp. 299–306, 2022. [Online]. Available: https://ijet.pl/index.php/ijet/article/view/10.24425-ijet.2022.139882
[15] S. P. Singh, S. R. Pendem, and D. Raveendhra, "A review on dc-dc converters for fuel cell electric vehicle applications," in *2024 IEEE Students Conference on Engineering and Systems (SCES)*, 2024, pp. 1–6.
[16] S. C. Mishra, L. Nanda, and B. Misra, "Review and comparison of DC-DC buck boost and boost converter topologies for fuel cell integration in electric vehicles and microgrids," in *2025 IEEE 1st International Conference on Smart and Sustainable Developments in Electrical Engineering (SSDEE)*. IEEE, pp. 1–7. [Online]. Available: https://ieeexplore.ieee.org/document/10968255/
[17] T. Koroglu, E. Ekici, and M. M. Savrun, "Five-port isolated bidirectional dc-dc converter for interfacing a hybrid photovoltaic–fuel cell–battery system with bipolar dc microgrids," *Electronics*, vol. 13, no. 6, 2024.
[18] R. Subbulakshmy, R. Palanisamy, S. Alshahrani, and C. A. Saleel, "Implementation of non-isolated high gain interleaved DC-DC converter for fuel cell electric vehicle using ANN-based MPPT controller," vol. 16, no. 3, p. 1335. [Online]. Available: https://www.mdpi.com/2071-1050/16/3/1335
[19] M. Forouzesh, Y. P. Siwakoti, S. A. Gorji, F. Blaabjerg, and B. Lehman, "High-efficiency high step-up dc–dc converters: A comprehensive review," *IEEE Transactions on Power Electronics*, vol. 32, no. 12, pp. 9143–9178, 2017.
[20] J. C. Rosas-Caro, J. M. Ramirez, and P. M. Garcia-Vite, "Novel dc-dc multilevel boost converter," in *2008 IEEE Power Electronics Specialists Conference*, 2008, pp. 2146–2151.
[21] J. Rosas-Caro, J. Ramirez, F. Peng, and A. Valderrabano, "A dc–dc multilevel boost converter," *IET Power Electronics*, vol. 3, pp. 129–137, 2010. [Online]. Available: https://digital-library.theiet.org/doi/abs/10.1049/iet-pel.2008.0253
[22] K. I. Hwu and Y. T. Yau, "An interleaved ac–dc converter based on current tracking," *IEEE Transactions on Industrial Electronics*, vol. 56, no. 5, pp. 1456–1463, 2009.
[23] Z. Wang, X. Su, N. Zeng, and J. Jiang, "Overview of isolated bidirectional dc–dc converter topology and switching strategies for electric vehicle applications," *Energies*, vol. 17, no. 10, 2024.
[24] R. Crews, "An-1820 LM5032 interleaved boost converter," Texas Instruments Incorporated, Application Report SNVA335A, May 2013, originally published May 2008; revised May 2013. [Online]. Available: https://www.ti.com/lit/an/snva335a/snva335a.pdf